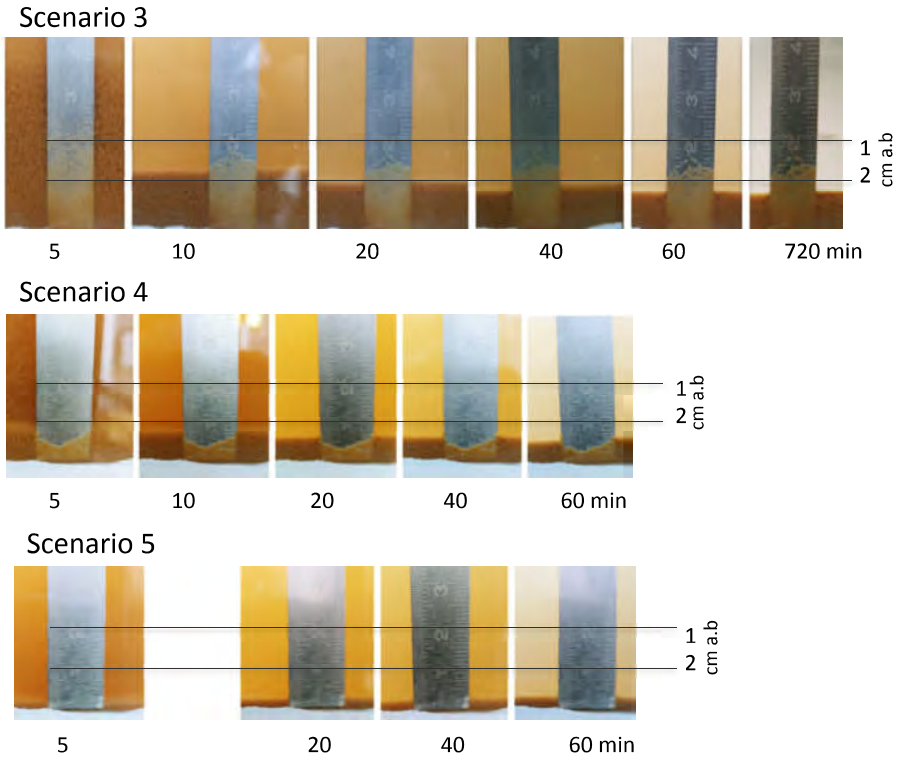

Fig. 13. Side view of test section of the flume showing the blanketing layer next to the window for better visualization. Note that a 3-4 mm have to be added to compensate for the silicone sealing next of the window. A-D is 5, 20, 60, 1440 minutes after release of the plume. For different concentrations of each scenario see Fig. 12.

E. Topographic analysis and quantification of the "Blanketing layer"

E.1 Original sample topographic analysis

The nodule field was scanned using an ADV Vectrino Profiler at (10Hz). Each scan took over 6 hours, and 200000 measuring points were collected. The final output results are presented in Fig. 14C. The use of an ADV over optical sensor such as a laser camera for 3D modeling of in-situ topography has revealed to be a powerful method and provides a new outlook for multi-usage of 3D sensors during mining activities.

The current resolution of the grid produced was X (0.47 mm), Y (1 mm), and Z (down to 10 µm). The output file (.ply) will be transferred to DG and can be easily opened with the open-source software MeshLab (www.meshlab.net; File --> Import Mesh). This will allow a 3D navigation inside the nodule field using the computer mouse.

Bottom elevation (Fig. 14B) determined by the 3D scan of the sediment surface revealed that the nodules created a microtopography which penetrated the bottom boundary layer [BBL] up to 16.8 mm with an average height of 8.6 ± 2.7 mm. Each nodule was placed into the sediment with the correct side up (hydrogenic nodule growth side) and embedded down to the mark showing the sediment water interface.

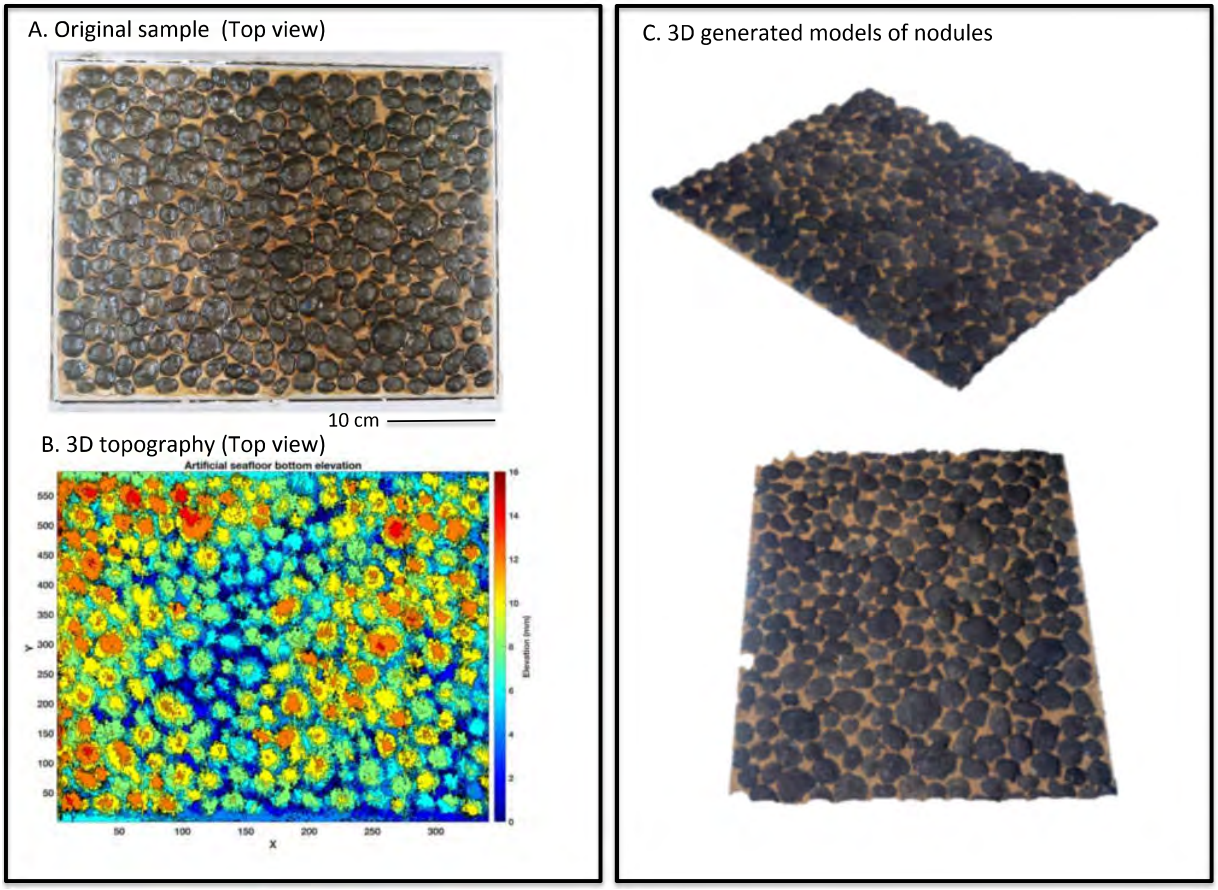

Fig. 14. 3D representation and microtopography of the Type 1 nodules.

E.2 Blanketing experiment

Fig. 15 shows the photograph and 3D map of the blanketing layer on the test section with Type 1 nodules after settling of a ≈ 1-meter height aggregated plume of 1 g/L (1000 g/m^3 see table 4, scenario 6). Bottom elevation (Fig.16 C) indicates that the topography of the nodule field has changed in comparison to the original sample (Fig.14 C). The Type 1 nodules were covered by a thin layer of plume particles and the microtopography surface became much smoother, as shown by both the pictures (Fig.15) and bottom elevation (Fig.16). All nodules were entirely covered by the deposited plume. Note that this occurs for any scenario with a blanketing layer of ≈ 11 mm (table 4, scenario 6). The shapes of the nodules are still visible under the newly formed sediment surface of the settled plume.

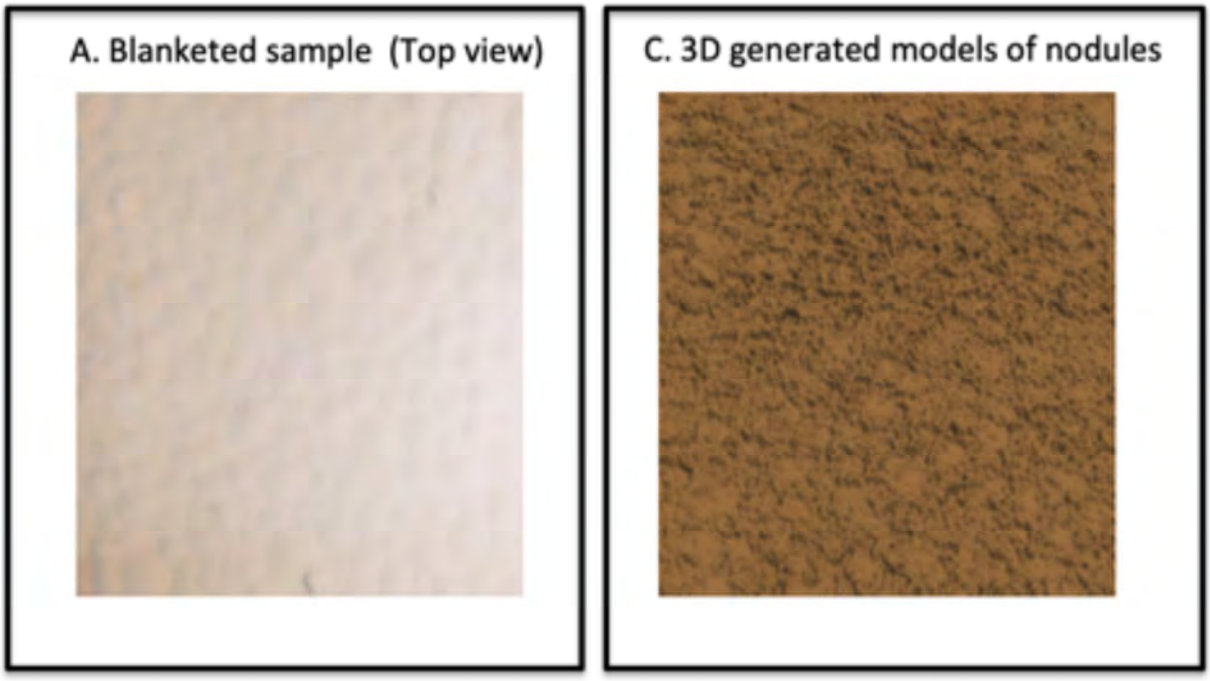

Fig. 15. Photography and 3D representation of the Type 1 nodule field.

A superposition between the original nodule's field and the newly formed blanketing layer is given in Fig. 17. Those results showed that the ADV sensor was able to precisely measure the newly form sediment bed and once more prove the efficiency of those instruments. The blanketing layer quantification was investigated based on a 3D cloud mesh comparison using the free software CloudCompare (See Method section). The blanketing thickness is shown as a color layer and plotted on the top of the original 3D grid of the Type 1 nodules for better visualization.

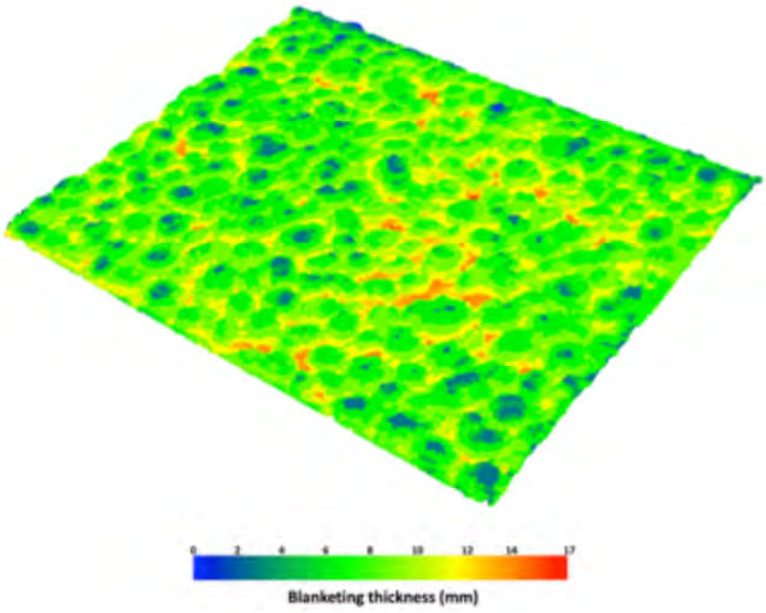

Fig. 16. Type 1 nodule blanketing thickness determined with the AV sensor. Average height of the Type 1 nodules into the benthic boundary layer was 8.6 ± 2.7 mm, with maximum height of 16 mm.

The average blanketing of the nodules ranged from 2 - 3.5 mm on top of nodules, which penetrated the BBL up to 16 mm to a blanketing layer of > 6 mm on top of smaller nodules. Decreasing nodule height (BBL penetration) resulted elevated blanketing. Increasing or decreasing the plume concentration will vary the blanketing layer accordingly.

E.3 Quantification of blanketing thickness

For the quantitative determination of the relationship between plume concentration at different heights above bottom [h.a.b] in g/m^3 dw (dry weight), the resulting sediment load on the seafloor (g/m^2) and the corresponding thickness of the blanketing layer (mm) three different approaches were used (Fig.17):
1. aggregated sediment plumes of known concentrations transferred by gravitation into test vials (series1, see fig. S3, p.27), 2. the isolated test section of the racetrack flume or 3. in water column simulator. The results are shown in Fig. 15 and table 4. The three different approaches resulted in very similar results. The blanketing layer thickness (mm) varied proportionally to the final accumulated sediment load (g/m^2) and allows to determine the blanketing effect of varying initial plume concentrations at different heights above the seafloor.

It is important to note that most data describe the blanketing up to a thickness of 16 mm, which would cover all Type 1 nodules at the NORI site. Higher blanketing loads are the result of high plume concentrations which would blanket and further compact. (see deviation from the linear regression lines presented in fig. 17 towards the green line which includes a 10 kg/m^3 blanketing effect).

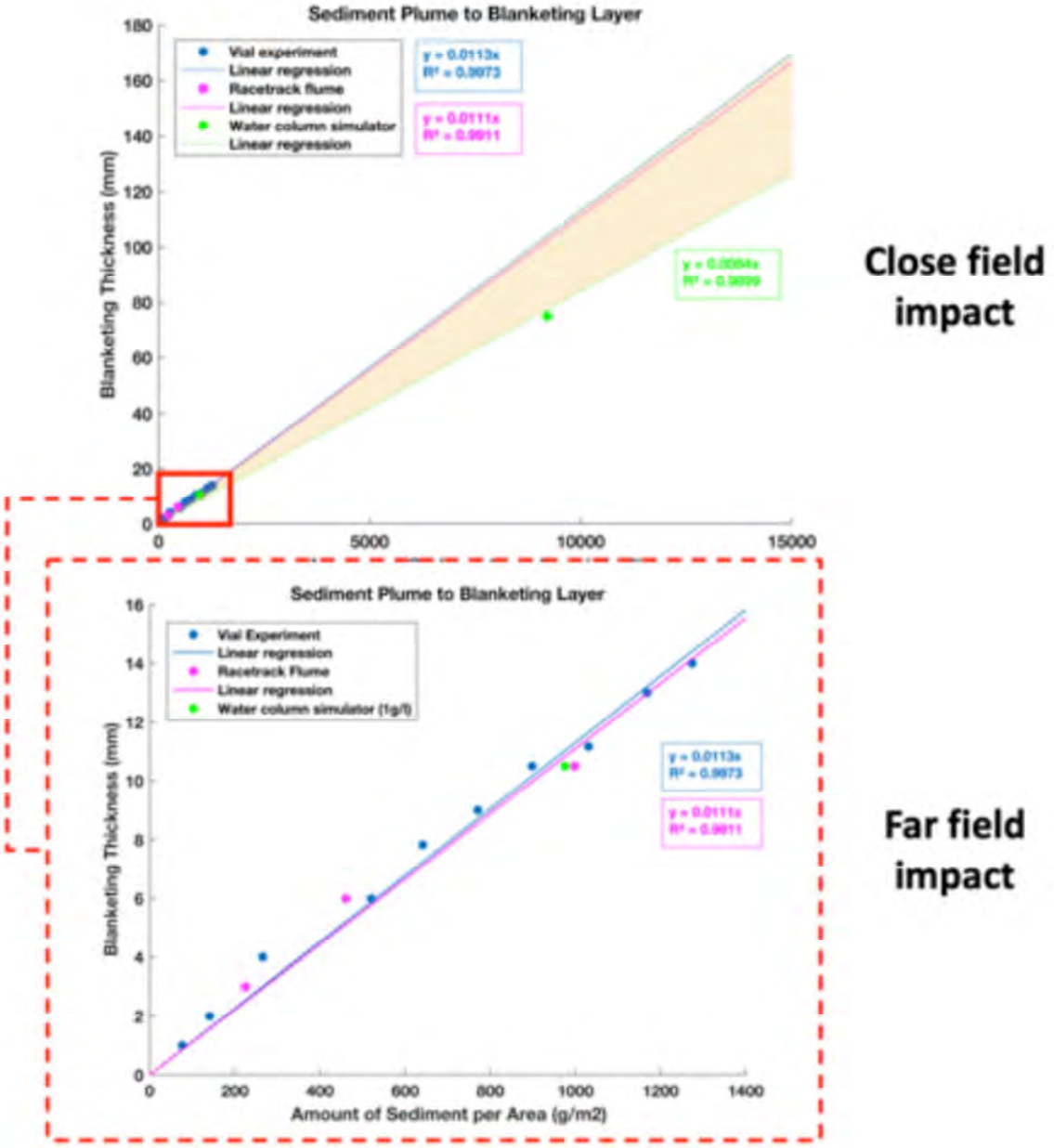

Fig. 17. Correlation between accumulated particle load on the seafloor and resulting thickness of the blanketing layer, as determined via three different experimental approaches.

Table 4. Thickness of the blanketing layer from different particle loads (g/m^2) on the seafloor using the correlation coefficients determined in Fig. 18 from the three different test scenarios.

[1]: 10 g/L plume concentrations at 1G in a 1 m water column (near field)
[2]: 0.03 g/L plume concentration in a 50 m water column (far field) or re-injection point
[3]: 0.01 g/L plume concentration in a 50 m water column (far field)
[4]: 0.01 g/L plume concentration in a 25 m water column (far field)
[5]: 1 g/L plume concentration in a 10 m water column (near field) or re-injection point
[6]: 1 g/L plume concentration in a 1 m water column (near field) or re-injection point

Blanketing [mm]	**g/m2 blanketing**	**g/m3 in water column**				
		1 m	**5m**	**10m**	**25m**	**50 m**
1	100	100	20	10	4	2
2	200	200	40	20	8	4
3	300	300	60	**30**	**12** [4]	6
5	400	400	80	40	16	8
6	500	500	100	50	20	**10** [3]
7	600	600	120	60	24	12
8	700	700	140	70	28	14
9	800	800	160	80	**32**	16
10	900	900	180	90	36	18
11	1000	**1000**[6]	200	**100**	40	20
12	1100	1100	220	110	44	22
14	1200	1200	240	120	48	24
15	1300	1300	260	130	52	26
16	1400	1400	280	140	56	28
17	1500	1500	300	150	60	**30** [2]
17	2000	2000	400	200	80	40
42	5000	5000	1000	500	200	**100**
84	10000	**10000** [1]	2000	**1000**[5]	400	200
420	50000	50000	10000	5000	2000	1000

F. Resuspension behavior under increasing flow conditions

Examples of the resuspension behavior of the blanketing layer after 12 or 48 hours of sedimentation on Type 1 nodules are presented in Fig. 18 under the three different scenarios (sc. 3,4,5; Fig. 12). Under flow conditions between 4 cm/s (0.1G, typical deep sea flow) and 15 cm/s (1G, simulation of a deep sea eddy) in sc.3, Fig 18, when the Type 1 nodules were completely covered by plume particles, no resuspension of the newly formed sediment surface took place. Only loose large aggregates which were not part on the original process of mud layer compaction were exported as bedload and suspended load. This would also be the case for an incoming flux or organic matter from the sea surface. The newly formed and almost flat sediment surface stayed intact.

Under sc.4 conditions of a thinner blanketing layer (Fig. 18) which still completely covered all Type 1 nodules (Fig. 18), erosion of the blanketing layer started at 9-10 cm/s at zones of enhanced turbulence either at the leading edgy of the nodule field and around only slightly covered nodules within the field. This erosion was further enhanced under flow velocities of 15 cm/s but did not result in large scale erosion of the blanketing layer during the following hours. Sc.4 represents a plume concentration of 500 g/m^3 in a 1 m water column or 10 g/m^3 in a 50 m water column (scenario [3] in table 4).

Under sc.5 conditions of an very thin blanketing layer (Fig. 18) which did not completely cover all Type 1 nodules (Fig. 18), erosion of the blanketing layer also started at 9-10 cm/s and was further enhanced under flow velocities of 15 cm/s, when an increasing number of larger Type 1 nodules were flushed and became visible again. Again, larger scale erosion of the blanketing layer did not occur during the following hours.
These results are different from type 2 and 3 nodules (as determined) for other projects, where large scale erosion around the nodules took place under these flow conditions of 15 cm/s.

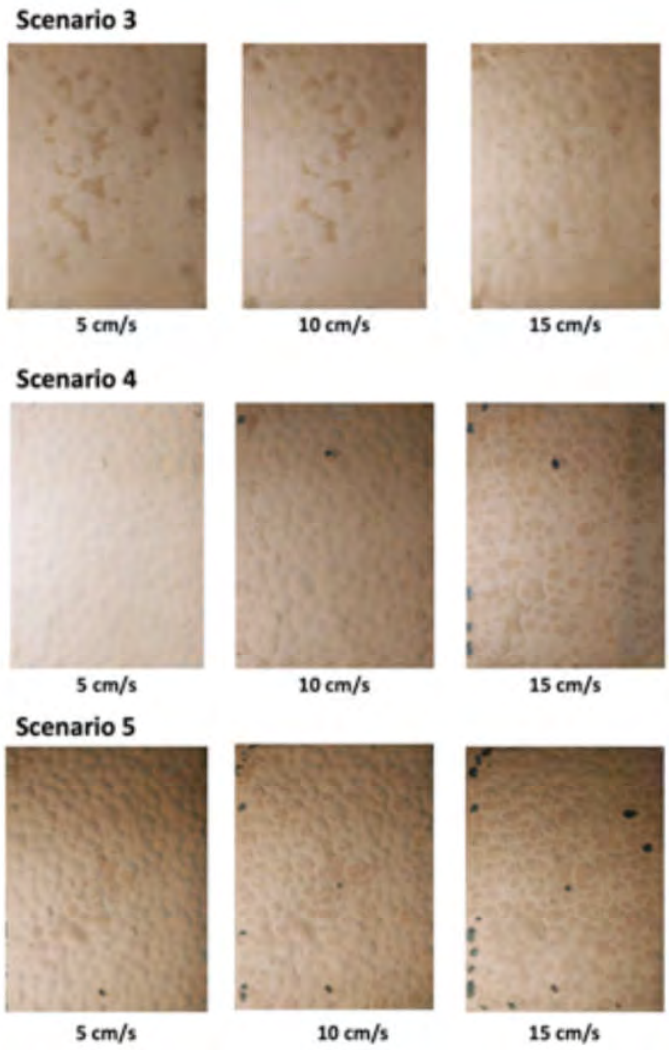

Fig. 18. Resuspension behavior of blanketing layer under increasing flow conditions and different blanketing heights Sc.3: 1 g/L, Sc.4: 0.5 g/L, Sc.5: 0.25 g/L to simulate conditions in a 1 m water column.

G. Flow field analysis of Type 1 nodules

The flow field model from Type 1 nodules under typical deep-sea flow conditions of 0.1 G (4 cm/s) was generated from 13,500 measuring points made with an ADV Vectrino sensor mounted on a 3D Isel arm. The same measuring grid was applied before and after the blanketing experiment for reliable comparison. The overall presentation of the flow field (Z component), including topography, is showed in Fig. 19.

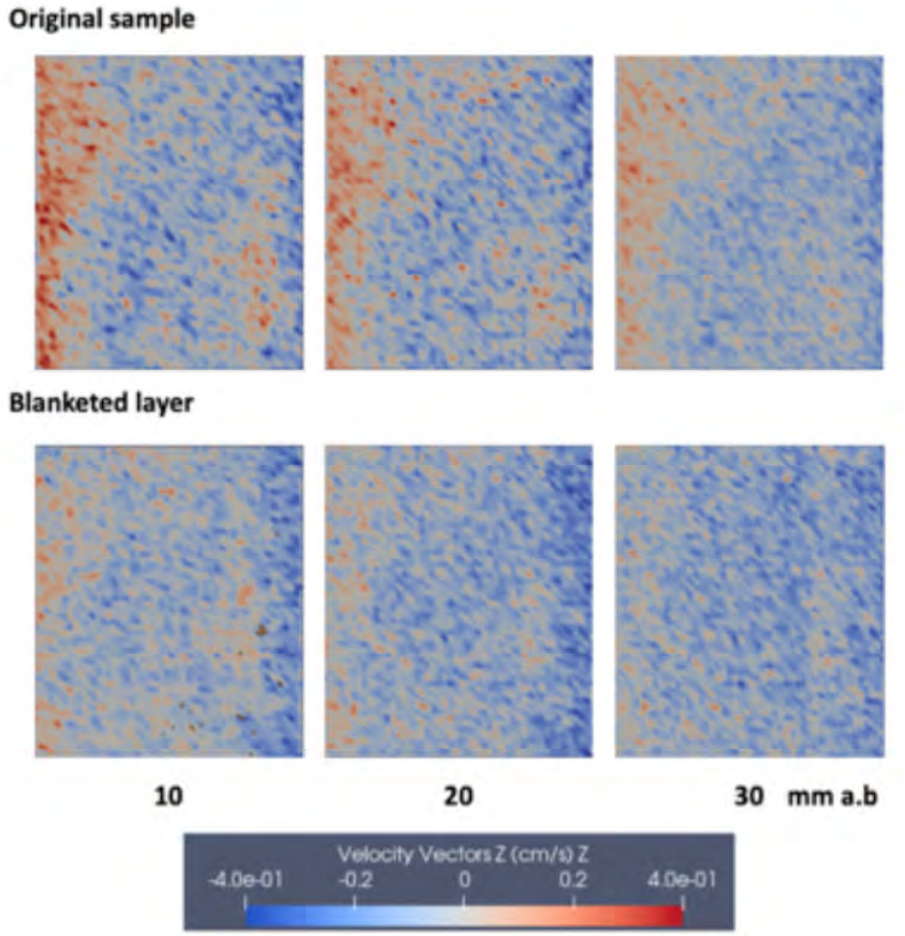

Fig. 19. Flow field comparison in Z direction of the Type 1 nodule test-bed. Flow direction: from left to right

For the original sample, a current deflection in the Z component (up to 0.4 cm/s upward) at the upstream (left) section of the model could be observed. This deflection develops, when deep sea currents enter a Type 1 nodule field and are deviated at the “leading edge” by the new micro-topography. The model also highlights the presence of abundant downward convergence cells (-0.1 to -0.4 cm/s; blue color), which are always associated with upward movement. From an ecological point of view, those observations are crucial. The turbulence is needed for benthic interface feeders to access food which would normally pass by. The turbulence above Type 1 nodules however is significantly lower than above Type 2 or 3 nodules.

After the blanketing, not only the topography had drastically changed (Fig.19, blanketed layer), but the convergence cells close to the seafloor have almost disappeared (Fig. 20B).

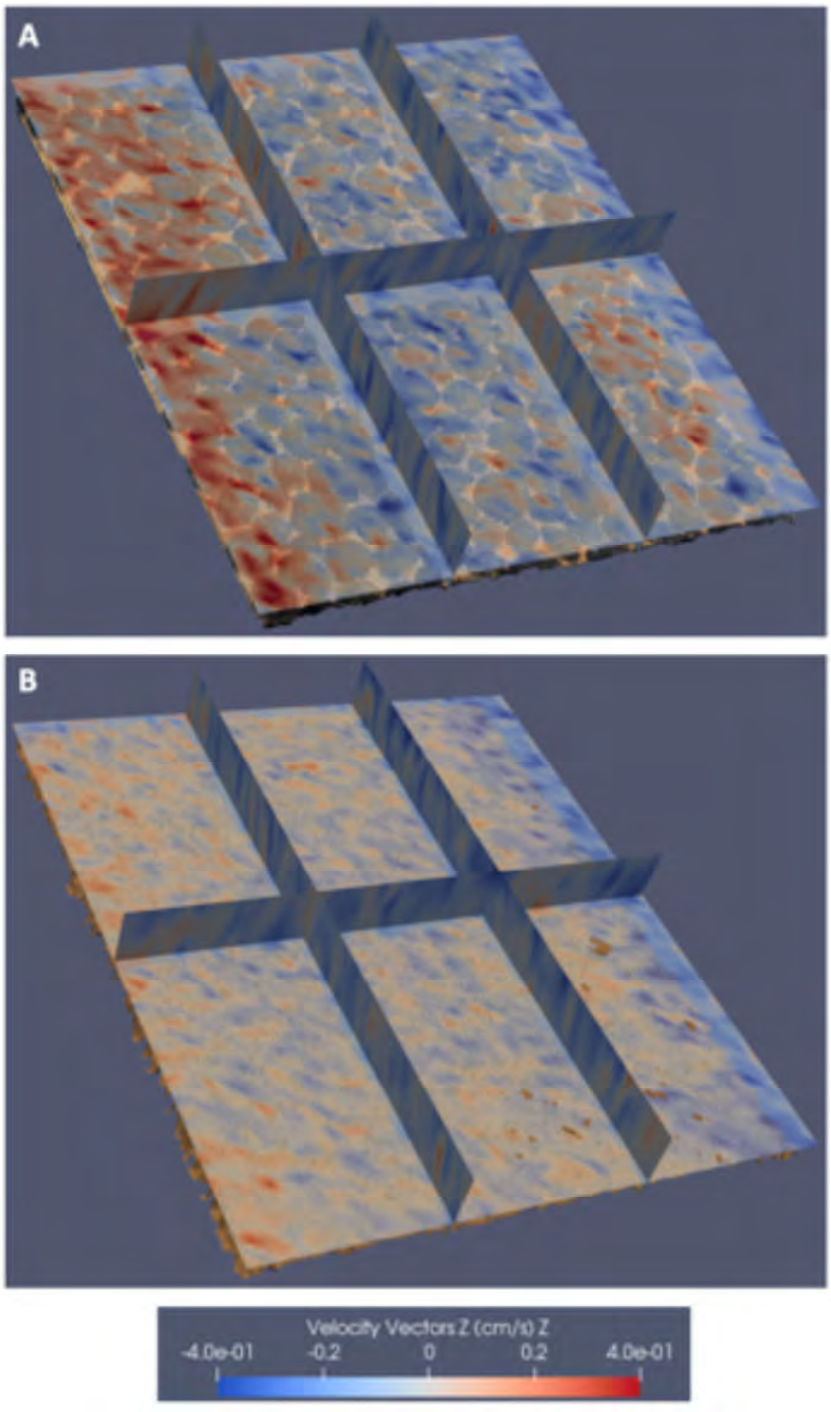

Fig. 20. Flow field measurement of Type 1 nodules. A: Original sample; B: After blanketing; Flow from left to right

Brief evaluation of the results for ecosystem functioning (L.Thomsen)

From an ecological point of view, decreasing water exchange within the BBL and increasing flow magnitude will impact the benthic communities. Benthic filter feeders, which have survived the blanketing episode, might therefore experience an organic matter depletion from the upper water column. This however will mainly take place in areas with Type 2 and 3 nodules where the change from original sediment surface to blanketed surface is much more pronounced, when a full blanketing took place. Small nodules create lower turbulence levels within the last centimeters above seafloor. The GIS map on nodule abundances in the NORI D site shows areas of ridges, troughs as well as flat landscapes. The geomorphology should have an influence on ecosystem functioning. Rougher terrain is more prominent in the Northern part of the Nori site. In trough landscapes megafauna showed the greatest variations in other studies. While regional CCZ benthic ecology has been suggested to be controlled by a gradient of POC flux to the seafloor local environmental factors presumably regulated by geomorphology, such as bottom water flows, nodule occurrence and xenophyophore test density may be important at the local scale. (Simon-Lledó et al. 2019).

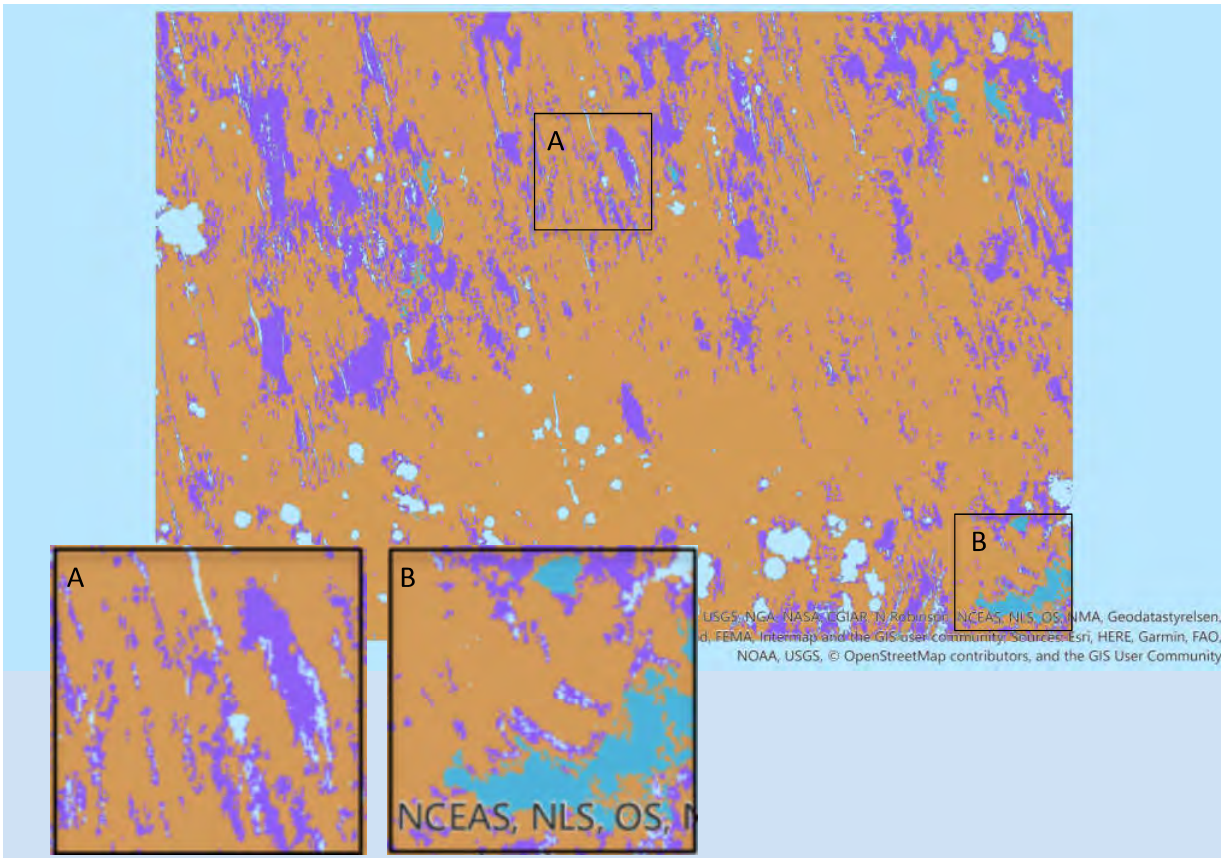

Fig. 21. GIS Map of NORI site, no scaling was provided. (approx. > 10 000 km^2)
Brown: Type 1 nodules
Purple: Type 2, 3 nodules
Light blue: Ridges and seamounts, rocky surfaces (strong backscatter)
Dark blue: valleys without nodules (M.Clarke per. Communication) or flat areas without nodules.

Low sedimentation rates or even a sedimentation interruption and the formation of an erosional surface may have provided suitable conditions for the formation of a great number of small particles which have acted as nuclei to start the growth of nodules. The larger hydrogenetic fraction of small-sized nodules indicates that they have generally formed under lower sedimentation rates compared to the larger nodules (Kuhn et al., 2020).

The importance of nodule abundance on megafaua and macrofauna

The following section discusses the current knowledge and some hypotheses. For the public perception the visible megafauna (> 2 cm in size) is important and shows the fragility and need for protection. For authorities as well as many scientists, macrofauna and megafauna are in focus of conservation initiatives (Danovaro,...Levin, ...Thomsen et al., 2020). To the best of the knowledge of the authors, there is no single ongoing, nor planned, monitoring strategy of a national agency based upon or prioritizing microbial or meiofaunal diversity in their standard protocols.

Macrofauna density **appeared** to increase with increasing nodule abundance in the seabed but to my knowledge, there is no study which **quantifies nodule size** with megafuaunal abundance and diversity. In my opinion, **megafauna** needs larger nodules as solid hard substrate for suspension feeding. The drag of even low deep sea currents would capsize a small nodule.

Fig. 22. (credit: Diva Amon and Craig Smith, Uni Hawaii)

Fig. 23. Small octopus wrapped itself around its eggs on the stabile stalk of a dead deep-sea sponge which was either attached to a larger nodule or deep within the sediment to avoid toppling.
(credit: Autun Purser, AWI OFOS team)

The hypothesis that larger nodules provide better substrate for megafauna is supported for example by a study on glacial dropstones enhancing seafloor species richness of benthic megafauna. These dropstones can be seen as example for the importance of larger nodules and as a suggestion how to restore biodiversity with larger hard substrate (stones). The study revealed a positive correlation between dropstone size and species richness, as well as an increase in the proportion of colonized dropstones with increasing dropstone size (Ziegler et al., 2017).

Personal communication with other experts on megafauna working in the CCZ in other joined projects further supported the idea that nodule size relates to megafauna abundance while high numbers of small nodule do not.

Current knowledge

The following summary presents short text passages from a workshop and a book chapter to present the current knowledge and assumptions:

Smith, C. R., et al. "Deep CCZ Biodiversity Synthesis Workshop Report." *International Seabed Authority (ISA). Friday Harbor, Washington* (2019)
And from the book chapter:
Kuhn, Thomas, et al. "Manganese nodule fields from the Northeast Pacific as benthic habitats." *Seafloor Geomorphology as Benthic Habitat*. Elsevier, 2020. 933-947.

• Megafauna play a significant role in deep-sea ecosystem function, in terms of phytodetritus consumption and bioturbation and carbon flow through the abyssal Pacific food web. Megafaunal density and morphotype richness were investigated in relation to modeled nodule abundance and POC flux to the

seafloor **but the biological data were of insufficient ranges for statistically robust trends to be drawn in some cases** (Kuhn et al., 2020)

• About 50% of all megafauna were shown to depend on nodules (Amon et al. 2016). While higher numerical densities have been observed in locations with higher nodule coverage of different sizes (Vanreusel et al., 2016), **the precise role of nodules and other local environmental factors in the ecology of CCZ megafauna is still poorly understood and based on relatively small areas sampled** (Simon-Lledó et al. 2019). Vanreusel et al. (2016) however, compared the area APEI3 with the BGR site North of NORI and concluded that POC flux is controlling Macro- and Megaufaunal abundances and not nodule abundance.

• Macrofauna is dominated by polychaets. The model explaining the most variance in mean polychaete abundance (numerical density) included POC flux and nodule abundance. The influence of POC flux was highly statistically significant **but the influence of nodule abundance was not**. Interestingly polychaete abundance seems rather negatively correlated with nodule abundance in some areas. Nodule abundance and depth, when assessed individually with Type II regression, exhibited weaker negative exponential relationships with polychaete abundance (Smith et al., p.85 of workshop report)

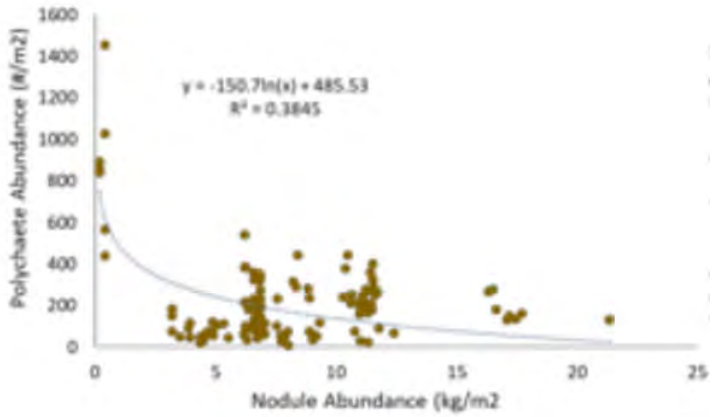

Fig. 24. Polychaet abundance versus nodules abundance (Smith et al., p.85 of workshop report)

Evironmental control and Ecosystem functions

Organic carbon input is considered as key variable for ecosystem functioning in the deep sea and SCOC (sediment community oxygen consumption) is an important parameter to analyze it (Danovaro et al., 2020), preferably on temporal and special scale.

• Multiple regression analysis on SCOC rates measured across the central Pacific revealed that POC flux was the only significant factor (p=0.006) affecting benthic respiration rather than nodule abundance for areas with little nodule abundance (< 10 kg/ m^{-2}). Therefore, relationships across a range of nodule coverage were

not possible to assess. **The authors cannot exclude the possibility that nodules may modify SCOC rates through their effect on bottom water current flow and particle and organic C deposition dynamics.** Temporal variability of SCOC and other ecosystem functions are needed; most studies encompass measurements made over hours to days. (Sweetman at al.,in Workshop report).

See also this iSeaMC report on flow fields around small nodules (Fig.20), and Simon-Lledó et al. (2019) on geomorphology.

• The highest densities, species richness and diversity were recorded in the Eastern part of the CCFZ (BGR license area), while the lowest values were found in the APEI3 area, which is rich in nodules but low in POC flux. The results correspond to the differences in productivity observed in the CCFZ (Błażewicz et al., 2019).

• Morphotype richness appeared to slightly increase with increasing nodule abundance but this relationship was weak and not statistically significant (r_S = 0.47, p > 0.05) (Jones et al., p 107 of workshop report). While higher numerical densities have been observed in locations with higher nodule coverage (Vanreusel et al., 2016), the precise role of nodules and other local environmental factors in the ecology of CCZ megafauna is still poorly understood and based on relatively small areas sampled (Simon-Lledó et al. 2019)

Nodule cover has previously been shown to be an important factor in the structuring of megafaunal communities (Simon-Lledó et al. 2019), as some taxa are known to require nodule habitat (Vanreusel et al. 2016, Amon et al 2016). However, these patterns are not necessarily linear. Simon-Lledó et al (2019) showed how local megafaunal densities increased describing a rapid asymptote (i.e. stabilising in mid-low nodule abundance levels) over a gradient of nodule coverage. This study also showed that local taxa richness appeared to be invariable across the nodule gradient unless this metric was calculated upon fixed-areal sampling units, as this effectively incorporated faunal density as a factor in the calculation of taxa richness.

Conclusion on nodule size and megafauna

I suggest that DG analyses many video transects from the Type 1 nodule sites to verify or falsify this hypothesis, combined with SCOC data in enhanced spatial and temporal resolution to quantify the flux of POC. Comparisons based on directly measured nodule abundance from seabed photographs to megafaunal density, also at regional scale, may be best suited to explore such patterns and will help DG to prepare for discussions with the public and authorities.

Comparison with other areas of the CCFZ

Median particle size in these top 15 cm of sediments was in the same range as those from other sites at the CCFZ (d_{50} of 8 to 25 µm respectively). The rapid aggregation within the first 30-60 minutes as well as the development of d_{50} of aggregates was also similar at other sampling sites. At all sites the export phase which resulted in a > 90 % deposition lasted between 60 and 120 m after the stop of release of the plume. Smaller

initial plume concentrations resulted in slower fallout times. This is consistent with results from experiments on concentrations < 500 mg with sediments further North of the NORI site. Compared to sites with higher d_{50} of the primary particles (eg 20 µm), the resulting settling velocities of the aggregates at the NORI D site were higher, most probably the result of denser packed aggregates of smaller original particles. Blanketing layer thickness at other locations under 0.5 and 1 g/L scenarios were in the same range.

Concluding remarks

Close collaboration with AllSeas should clarify the expected range of particle concentrations -and size at the midwater injection point and behind the collector. Then modeling of plumes will give best estimates of the impact areas.

Following the suggestions of Mingotti and Woods (2020) the plume would create a water layer of enhanced particle concentration where turbulent aggregation will result in rapid vertical export; or turbulent dispersal is so strong that aggregation is prevented and fine particles are diffusing into the deep Pacific as suggested by others. Results from Dredging should give insights into that process. For deep sea mining activities, there is only one short video sequence from MIT available, which indicates particle fallout. In accordance with Mingotti and Woods (2020) we assume that the flow is turbulent which support aggregation and the particles and fluid descend to the level at which the bulk speed of the flow falls to zero. After an initial overshoot, the flow begins to spread laterally at its neutral buoyancy level. There is then a zone of fluid–particle separation, with particles falling down while the residual fluid becomes more buoyant (see Fg. 4, Mingotti and Woods, 2020). We assume midwater concentrations of ≈ 10 g/L now and nodule fines which might modify aggregation.

Same holds true for the exhaust pipe behind the collector. The plume will descent down to the seafloor and aggregation will take place. Data with real expected concentrations should be used for experiments. We assume concentrations of > 40 g/L now. The fluid mud layer will rapidly produce hindered settling or even gelling. An injection of nodule fines might change the transport behavior of these highly concentrated fluid muds before. Only those data will provide best prerequisites for reliable prognosis, before a collector test will give real answers to these important questions.

iSeaMC can discuss the results of this report with the DG Modelers to decide on the best suited particle characteristics for the current midwater and seafloor injection points.

Additional figures

Fig. S1. Incoming gravity flow under 0.1 G conditions in the seawater flume

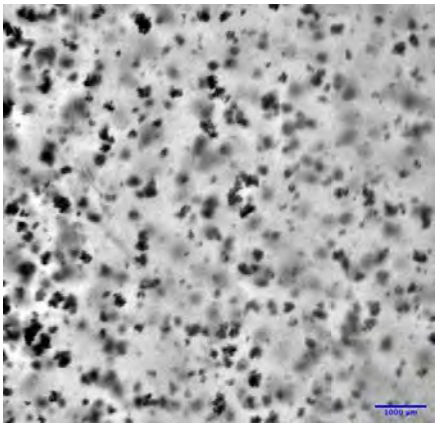

Fig. S2. Suspended aggregates during aggregation of 1 g/L sediment plume at 60 min

Fig. S3 Test vials for fig. 15. Aggregated plume particles were inserted to determine the height of the resulting mud layer

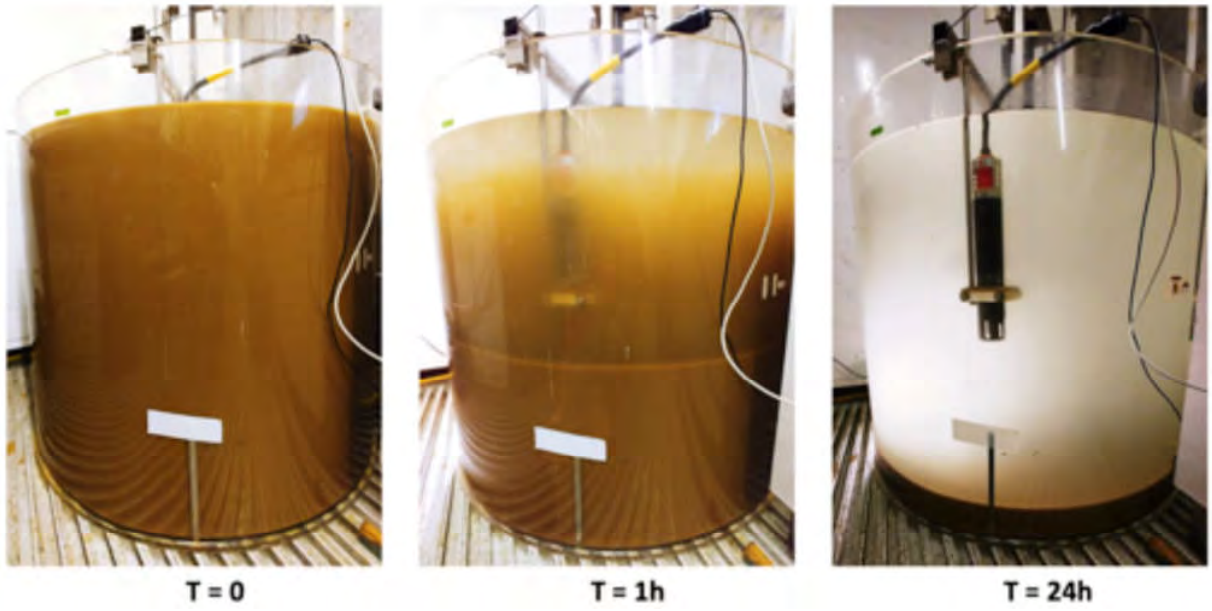

Fig. S4. Development of the fluid mud layer. T0 under 10 g/l, T1 during the export phase of newly formed aggregates which form a unconsolidated mud layer, T24: 1 day after plume release and 22 h after the export phase ended, when the mud layer is consolidated and remaining fine particles < 100 µm will create a new sediment surface.

Fig. S5. Plume aggregates during deposition (0.6 mm: compaction area ; 6 - > 40 mm: agglomeration) in the flume

G. References:

Ahrens, James, Geveci, Berk, Law, Charles, ParaView: An End-User Tool for Large Data Visualization, Visualization Handbook, Elsevier, 2005, ISBN-13: 978-0123875822

Amon, D.J., Ziegler, A.F., Dahlgren, T.G., Glover, A.G., Goineau, A., Gooday, A.J., et al., 2016. Insights into the abundance and diversity of abyssal megafauna in a polymetallic-nodule region in the eastern Clarion- Clipperton Zone. Sci. Rep. 6, 30492.

Błażewicz, Magdalena, et al. "High species richness and unique composition of the tanaidacean communities associated with five areas in the Pacific polymetallic nodule fields." Progress in Oceanography 176 (2019): 102141.

Dankers, P. J. T., and J. C. Winterwerp. "Hindered settling of mud flocs: theory and validation." Continental shelf research27.14 (2007): 1893-1907.

Danovaro, R., Fanelli, E., Aguzzi, J., Billett, D., Carugati, L., Corinaldesi, C., ...Levin, L.,..Thomsen, L., . & McClain, C. (2020). Ecological variables for developing a global deep-ocean monitoring and conservation strategy. Nature Ecology & Evolution, 4(2), 181-192.

Garcia, R., and L. Thomsen. "Bioavailable organic matter in surface sediments of the Nazaré canyon and adjacent slope (Western Iberian Margin)." Journal of Marine Systems 74.1-2 (2008): 44-59.

Gardner, Wilford D., Mary Jo Richardson, and Alexey V. Mishonov. "Global assessment of benthic nepheloid layers and linkage with upper ocean dynamics." *Earth and Planetary Science Letters* 482 (2018): 126-134.

Gillard, B. , Purkiani, K. , Chatzievangelou, D. , Vink, A. , Iversen, M. and Thomsen, L. (2019): Physical and hydrodynamic properties of deep sea mining-generated, abyssal sediment plumes in the Clarion Clipperton Fracture Zone (eastern-central Pacific) , Elementa, 7 (1) . doi: 10.1525/elementa.34

Hill, P.S., Nowell, A.R.M., 1990. The potential role of large, fast sinking particles in clearing nepheloid layers. Philosophical Transactions of the Royal Society of London Series A 331, 103}117.

Hill. P.S. Newgard. J.P.. Law. B.A.. Milligan. T.G.. (2013). Flocculation on a Muddy Intertidal Flat in Willapa Bay. Washington. Part II: Observations of Suspended Particle Size in a Secondary Channel and Adjacent Flat. Continental Shelf Research.

Jackson, G. A. (2015). Coagulation in a rotating cylinder. Limnology and Oceanography: Methods, 13(4), 194-201.

Kuhn, Thomas, et al. "Manganese nodule fields from the Northeast Pacific as benthic habitats." Seafloor Geomorphology as Benthic Habitat. Elsevier, 2020. 933-947.

Mikkelsen. O.. P. S. Hill. T. Milligan. and R. Chant (2005). In situ particle size distributions and volume concentrations from a LISST-100 laser particle sizer and a digital floc camera. Cont. Shelf Res.. 25. 1959–1978.

Mingotti, Nicola, and Andrew W. Woods. "Stokes settling and particle-laden plumes: implications for deep-sea mining and volcanic eruption plumes." Philosophical Transactions of the Royal Society A 378.2179 (2020): 20190532.

R. G. A. Craig, C. Loadman, B. Clement, P. J. Rusello and E. Siegel, "Characterization and testing of a new bistatic profiling acoustic Doppler velocimeter: The Vectrino-II," 2011 IEEE/OES 10th Current, Waves and Turbulence Measurements (CWTM), Monterey, CA, 2011, pp. 246-252. doi: 10.1109/CWTM.2011.5759559

Sanford LP (1997) Turbulent mixing in experimental ecosystem studies. Mar Ecol Prog Ser 161:265–293

Simon-Lledó, E., Bett, B.J., Huvenne, V.A., Schoening, T., Benoist, N.M., Jeffreys, R.M., Durden, J.M. and Jones, D.O., 2019. Megafaunal variation in the abyssal landscape of the Clarion Clipperton Zone. Progress in oceanography, 170, pp.119-133.

Smith, C. R., et al. "Deep CCZ Biodiversity Synthesis Workshop Report." International Seabed Authority (ISA). Friday Harbor, Washington (2019)

Stolzenbach, K.T., Elimelech, M., 1994. The e!ect of particle density on collisions between sinking particles: implication for particle aggregation in the ocean. Deep-Sea Research I 41 (3), 469}483.

Thomsen L, McCave IN (2000) Aggregation processes in the benthic boundary layer at the Celtic Sea continental margin. Deep-Sea Research I, 47, 1389-1404.

Thomsen. L.. Gust. G.. 2000. Sediment erosion thresholds and characteristics of resuspended aggregates on the western European continental margin. Deep Sea Research Part I: Oceanographic Research Papers 47. 1881–1897.

Tinevez, JY.; Perry, N. & Schindelin, J. et al. (2017), "TrackMate: An open and extensible platform for single-particle tracking.", Methods 115: 80-90, PMID 27713081

Tran, Duc, Rachel Kuprenas, and Kyle Strom. "How do changes in suspended sediment concentration alone influence the size of mud flocs under steady turbulent shearing?." Continental Shelf Research 158 (2018): 1-14.

Vanreusel, A., Hilario, A., Ribeiro, P. A., Menot, L., & Arbizu, P. M. (2016). Threatened by mining, polymetallic nodules are required to preserve abyssal epifauna. Scientific reports, 6, 26808.

Ziegler, A. F., et al. "Glacial dropstones: islands enhancing seafloor species richness of benthic megafauna in West Antarctic Peninsula fjords." Marine Ecology Progress Series583 (2017): 1-14.

Smith, C. R., et al. "Deep CCZ Biodiversity Synthesis Workshop Report." International Seabed Authority (ISA). Friday Harbor, Washington (2019)

And from the book chapter: